nature nanotechnology

LETTERS

PUBLISHED ONLINE: 4 APRIL 2016 | DOI: 10.1038/NNANO.2016.49

Electrical generation and control of the valley carriers in a monolayer transition metal dichalcogenide

Yu Ye[1], Jun Xiao[1], Hailong Wang[2], Ziliang Ye[1], Hanyu Zhu[1], Mervin Zhao[1], Yuan Wang[1], Jianhua Zhao[2], Xiaobo Yin[3] and Xiang Zhang[1,4,5]*

Electrically controlling the flow of charge carriers is the foundation of modern electronics. By accessing the extra spin degree of freedom (DOF) in electronics, spintronics allows for information processes such as magnetoresistive random-access memory[1]. Recently, atomic membranes of transition metal dichalcogenides (TMDCs) were found to support unequal and distinguishable carrier distribution in different crystal momentum valleys. This valley polarization of carriers enables a new DOF for information processing[2–4]. A variety of valleytronic devices such as valley filters and valves have been proposed[5], and optical valley excitation has been observed[2–4]. However, to realize its potential in electronics it is necessary to electrically control the valley DOF, which has so far remained a significant challenge. Here, we experimentally demonstrate the electrical generation and control of valley polarization. This is achieved through spin injection via a diluted ferromagnetic semiconductor and measured through the helicity of the electroluminescence due to the spin–valley locking in TMDC monolayers[6]. We also report a new scheme of electronic devices that combine both the spin and valley DOFs. Such direct electrical generation and control of valley carriers opens up new dimensions in utilizing both the spin and valley DOFs for next-generation electronics and computing.

Inversion symmetry breaking together with spin–orbit coupling leads to coupled spin and valley physics in TMDC monolayers, which allows the charge carrier's valley DOF to be accessed via spin injection. TMDC monolayers possess direct energy gaps located at the unequal K and K′ valleys in the reciprocal space (Fig. 1a). At these valleys, the strong spin–orbit interaction originating from the transition metal ion's d orbitals introduces a large split in the valence bands. For example, the split can be up to ~440 meV in a tungsten disulfide (WS_2) monolayer[7–9]. The spin projection along the c axis of the monolayer crystal, S_z, is well defined and the two split bands are spin-up and spin-down[4,6]. In consequence, the respective time-reversal symmetry requires that the spin splitting must be opposite at the two distinct valleys, leading to a spin–valley locking relationship. The intravalley scattering is unlikely to be due to the large valence band edge splitting, as intervalley scattering involves a simultaneous spin flip, which is suppressed due to the large momentum mismatch. The transitions between split valence and conduction band edges are excitonic in nature, termed the A and B excitons[10,11]. Valley-contrasting optical selection rules are therefore expected due to the spin–valley locking in TMDC monolayers. This locking relationship and the large valence band splitting strongly suppress the spin and valley scattering[6], leading to a long valley-spin lifetime in TMDC monolayers[4,12].

Using the long-lived spin and valley DOFs, we electrically pump and confine the carriers in one set of the two distinct valleys (K or K′) through specific spin injection. As the spin splitting of TMDCs is manifested in the out-of-plane direction[13], we employed a ferromagnetic semiconductor with an out-of-plane magnetic easy axis as a spin aligner (Fig. 1b). Circularly polarized electroluminescence forming at the heterojunction between the heavily doped p-type (Ga,Mn)As and n-type monolayer WS_2 at forward bias was captured as the measured signal, caused by the unbalanced spin injected carrier population at K and K′ valleys. The (Ga,Mn)As is lithographically defined into a mesa shape, and an exfoliated WS_2 monolayer is mechanically transferred to the edge of the mesa. To prevent substrate leakages, a thin film of SiO_2 is deposited and patterned to provide good electric isolation between the monolayer and the substrate. An In/Au (10/80 nm) electrode is then introduced to form an ohmic contact on the monolayer WS_2 (see Supplementary Section Ia). It is worth noting that we have developed a site-specific dry transfer technique that allows precise placement of the exfoliated monolayer WS_2 and simultaneously provides a clean interface between the monolayer and the ferromagnetic semiconductor, which is crucial for spin injection (see Supplementary Section Ib). When a forward bias is applied on the (Ga,Mn)As, with the In/Au electrode grounded, the injection of holes from (Ga,Mn)As across the junction gives rise to efficient radiative recombination due to the direct bandgap of monolayer WS_2. The large concentration of electrons in the monolayer WS_2 is mostly introduced by localized sulfur vacancies[14]. The corresponding electroluminescence has been used as a reliable way to study optical transitions in monolayer TMDCs[15–19]. The electrical valley polarization can be directly determined from the helicity of the emitted electroluminescence as a result of the valley-resolved recombination between the electrically injected spin-polarized holes and the selected unpolarized electrons in monolayer TMDC due to preservation of valley-contrasting selection rules.

A representative current–voltage for the n-WS_2/p-(Ga,Mn)As heterojunction shows clear rectifying behaviour (Fig. 2a). The electroluminescence is localized at the edge of the heterojunction (inset of Fig. 2a), as the largest voltage drop naturally occurs across the heterojunction edge due to the semiconducting nature

[1]NSF Nanoscale Science and Engineering Center, University of California, 3112 Etcheverry Hall, Berkeley, California 94720, USA. [2]State Key Laboratory of Superlattices and Microstructures, Institute of Semiconductors, Chinese Academy of Sciences, PO Box 912, Beijing 10083, China. [3]Department of Mechanical Engineering and Materials Science and Engineering Program, University of Colorado Boulder, Boulder, Colorado 80309, USA. [4]Materials Sciences Division, Lawrence Berkeley National Laboratory, 1 Cyclotron Road, Berkeley, California 94720, USA. [5]Department of Physics, King Abdulaziz University, Jeddah 21589, Saudi Arabia. *e-mail: xiang@berkeley.edu

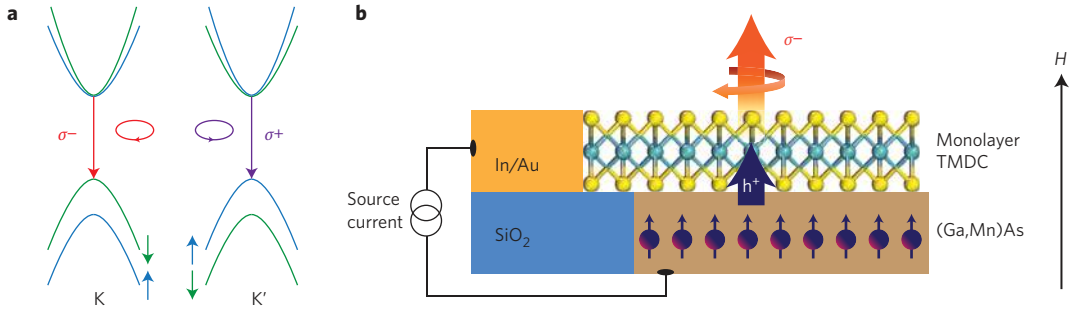

Figure 1 | Electrically driven valley polarization via spin injection and the principle of operation. a, Electronic structure at the K and K′ valleys of monolayer TMDC. K and K′ represent the two distinct momentum valleys in the reciprocal space of a TMDC monolayer. The spin degeneracy at the valence band edges is lifted by spin–orbit interactions. Electrical excitation and confinement of the carriers in one set of the two non-equivalent valleys are achieved through the manipulation of the injected carrier spin polarizations, due to the spin–valley locking in monolayer TMDCs. Optical selection rules give rise to opposite circularly polarized light emissions at different excited valleys. **b**, Schematic of the monolayer TMDC/(Ga,Mn)As heterojunction for electrical valley polarization devices. (Ga,Mn)As was used as a spin aligner under an external magnetic field. The valley polarization can be directly determined from the helicity of the emitted electroluminescence as a result of the recombination between the electrically injected spin-polarized holes and the selected degenerate electrons in TMDC monolayers.

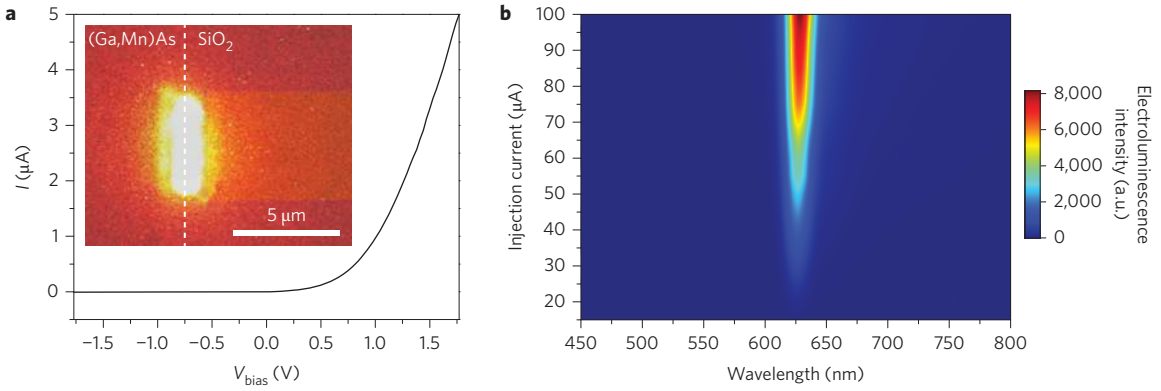

Figure 2 | Electroluminescence of the monolayer WS_2/(Ga,Mn)As heterojunctions. a, Electrical characteristics of the WS_2 diode, showing clear rectifying behaviour for bias voltage between –1.5 to +1.5 V. Inset: Surface plot of the electroluminescent emission overlaid with the scanning electron micrograph image at a forward bias of 5 V. The electroluminescence is localized at the edge of heterojunction. By applying an in-plane bias voltage, the largest voltage drop naturally occurs across the heterojunction edge due to the semiconducting characteristics of monolayer WS_2. The white dashed line indicates the interface between the SiO_2 and (Ga,Mn)As film. **b**, Electroluminescence intensity of the WS_2/(Ga,Mn)As heterojunction as a function of injection current and emission photon wavelength. The strong electroluminescence resonance peak at 1.97 eV (A exciton) is clearly observed and increases with the carrier injection rate. No B exciton and defect-related emission features are observed.

of monolayer WS_2 (see Supplementary Section IIa). The devices were mounted in an optical cryostat where the electroluminescence is captured by a 50× (numerical aperture = 0.55) long-working-distance objective. A strong electroluminescence resonance peak at 1.97 eV is noticeable (Fig. 2b) when the injection current exceeds 15 μA, corresponding to an applied voltage of 3 V. The electroluminescence intensity increases with the carrier injection rate, and the central emission wavelength and linewidth have a slight red shift and broadening, respectively, at a higher injection current due to Joule heating. No defect-related emission is observed, indicating the high quality of the monolayer WS_2. Owing to the electrical isolation of the SiO_2 layer, the emission from the monolayer WS_2 is the only feature of the observed electroluminescence (see Supplementary Section IIb). We note that the electroluminescence spectra do not show a measureable B exciton complex in the monolayer WS_2/(Ga,Mn)As junction, which differs from those of monolayer MoS_2/(Ga,Mn)As and $MoSe_2$/(Ga,Mn)As heterojunctions (see Supplementary Section IIc). The strong suppression of the B exciton emission in a WS_2/(Ga,Mn)As heterojunction, conducive to the electrical valley confinement, is a result of the large valence band splitting (~440 meV) of monolayer WS_2. The large valence splitting prevents the high-energy holes from populating the B exciton band, resulting in only the A exciton complex being observed in the electroluminescence spectra (Fig. 2b). In contrast, the valence splitting of monolayer MoS_2 (refs 5,20) and $MoSe_2$ (refs 21,22) are much smaller, approximately 160 meV and 180 meV, respectively, which allows a certain population of the B exciton emissions in monolayer MoS_2- and $MoSe_2$-based heterojunctions. Moreover, non-negligible defect-related emission was observed for MoS_2/(Ga,Mn)As heterojunctions due to the intrinsic defects of natural molybdenites[23].

Because A and B excitons possess opposite spin indices at different valleys (K and K′), the isolation of A and B excitons allows us to spectroscopically detect the valley population by observing the valley-polarized electroluminescence via manipulating the spin indices of the charge carriers. The ferromagnetic (Ga,Mn)As semiconductor serves as a natural spin aligner and allows spin-polarized hole injection. Using a ferromagnetic semiconductor for spin injection into a nonmagnetic semiconductor has the unique advantages of conductivity matching and thus the high spin injection efficiency[24–26]. The Curie temperature and coercivity at 5 K of the (Ga,Mn)As films with an effective Mn concentration of 5.9% are about 150 K and 200 Oe, respectively[27] (see Supplementary Section III). The in-plane tensile strained (Ga,Mn)As films are

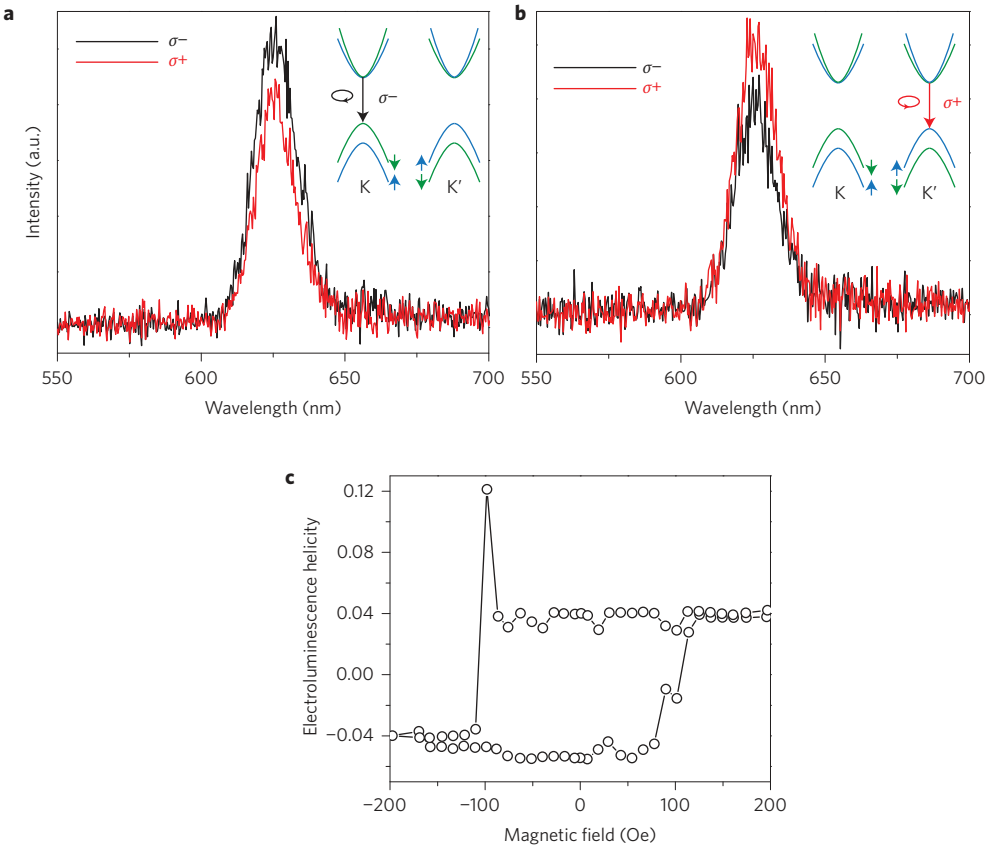

Figure 3 | Electrical control of valley polarization in monolayer WS_2. Spectra of **a**, $\sigma-$ and $\sigma+$ resolved electroluminescence polarized under an outward magnetic field of 400 Oe perpendicular to the surface with a current of 15 μA. The electroluminescence helicity, $\rho = (I_{\sigma-} - I_{\sigma+})/(I_{\sigma-} + I_{\sigma+})$, is found to be as large as 16.2% at the peak, indicating strong valley polarization in the monolayer WS_2/(Ga,Mn)As heterojunction as a result of spin-polarized hole injections. Inset: Schematic representation of electrical excitation and emission processes. The K valley is populated by spin-up hole injection from spin-polarized (Ga,Mn)As due to spin–valley locking, resulting in $\sigma-$ light emission as a result of the optical selection rules. **b**, Spectra of $\sigma-$ and $\sigma+$ resolved electroluminescence polarized under an inward magnetic field of 400 Oe perpendicular to the surface. An opposite electroluminescence helicity of $\rho = -14.8\%$ is observed. Inset: Schematic representation of electrical excitation and emission processes. The reversed magnetic field allows injection of the opposite (spin-down) holes and populating the inversed valley, K′, resulting in $\sigma+$ light emission. **c**, Out-of-plane magnetic field dependence of electroluminescence helicity of a new device operated at 10 K with a current of 30 μA. The helicity of the electroluminescence has a hysteresis loop that agrees with the SQUID magnetometer and anomalous Hall effect measurement. The clear squared hysteresis of electroluminescence helicity confirms the electrical generation of valley polarization. Spin switching causes a zero intensity difference in the $\sigma-$ and $\sigma+$ light emission. As the lock-in amplifier cannot detect the signal, a large outlier occurs at –100 Oe.

perpendicularly magnetized, which is coherent with the S_z spin in monolayer TMDCs. By applying an external magnetic field, we polarize the injected holes from the (Ga,Mn)As films that match in one of these two distinct valleys (K and K′). In other words, the momentum of the populated valleys is uniquely determined by the spin polarization of the injected holes. Subsequently, the electroluminescence from the heterojunctions is therefore expected to be valley polarized, governed by the injected spin polarization due to the unique spin valley locking.

The degree of valley polarization from a heterojunction of a TMDC monolayer and ferromagnetic semiconductor is determined from the polarization helicity of the electroluminescence. A Helmholtz coil with a maximum magnetic field of 400 Oe normal to the sample surface was used to polarize the hole carriers in the ferromagnetic semiconductor. The injection of spin-polarized holes leads to the carrier population in a specific momentum valley due to the spin valley locking in monolayer TMDCs, giving rise to circularly polarized light emission. When injecting spin-up holes with a magnetic field pointing outward towards the sample, the K valley is populated (inset of Fig. 3a), leading to right-circularly polarized light emission, and vice versa. Because the B excitonic feature in the n-WS_2/p-(Ga,Mn)As heterojunction is substantially suppressed, we focus on the A excitonic feature. Under an outward magnetic field perpendicular to the surface, we present the polarization-resolved electroluminescence spectra ($\sigma-$ and $\sigma+$ components) of the monolayer WS_2-based heterojunction at 15 μA (Fig. 3a). The electroluminescence helicity, $\rho = (I_{\sigma-} - I_{\sigma+})/(I_{\sigma-} + I_{\sigma+})$, is found reach a maximum at 16.2%, indicating the strong valley polarization in the monolayer WS_2/(Ga,Mn)As heterojunction as a result of spin-polarized hole injections. Here $I_{\sigma-}$ and $I_{\sigma+}$ are the energy-integrated intensities of the right- and left- circularly polarized electroluminescence, respectively. We observe a decrease in the helicity of the electroluminescence when the injection current is increased due to an increase in local temperature from Joule heating at high injection currents. It is suspected that phonon-assisted intervalley relaxation and intervalley electron–hole exchange interactions may play a role in defining the degree of helicity at a high injection current[28,29]. Another possibility is a surface oxidation layer on the (Ga,Mn)As[30] that results in a tunnelling barrier in the heterojunction, reducing the spin injection efficiency under high injection currents. Further studies are needed to clarify these issues. When an inward magnetic field is applied, an opposite electroluminescence helicity of $\rho = -14.8\%$ is observed as the reversed magnetic field allows injection of the opposite (spin-down) holes and population of the opposite valley, K′ (Fig. 3b). The electrical generation of valley polarization is further

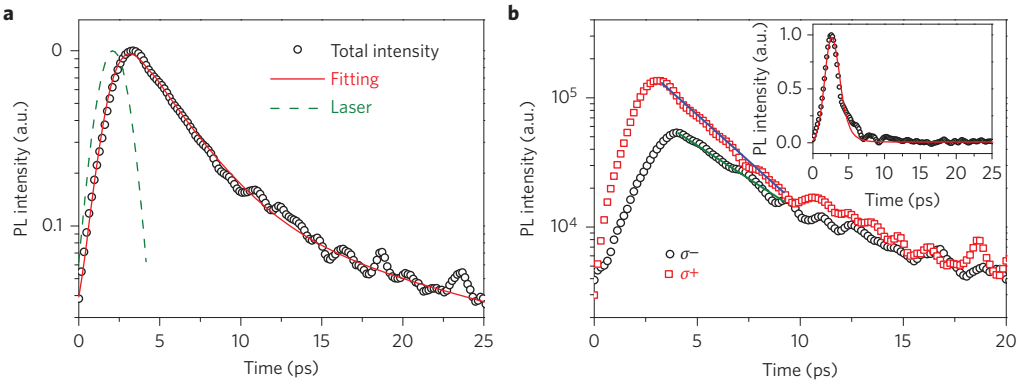

Figure 4 | Valley dynamics measurement in monolayer WS_2 on (Ga,Mn)As. a, Time-resolved total photoluminescence using a σ+ polarization femtosecond excitation laser pulse with an energy of 2.21 eV. Convolution fitting with the laser pulse (green dashed line), yields two exciton lifetimes of 2.9 ps and 20.0 ps. **b**, Time-resolved σ+ and σ– photoluminescence components excited by a σ+ polarized laser. Blue and green lines indicate the different decay rates for these two components. Inset: Convolution fitting (red curve) for the time-resolved valley exciton population (σ+ – σ–, black circles). The intervalley scattering time is estimated to be 2.5 ps.

confirmed by the magnetic field dependence of the electroluminescence helicity (see Supplementary Section IV), which shows clear squared hysteresis (Fig. 3c), agreeing with the SQUID magnetometer and anomalous Hall effect measurements. To confirm that the observed electroluminescence polarization is not due to magnetic circular dichroism (MCD) of the (Ga,Mn)As films or the Zeeman effect from the applied magnetic field, we performed polarization-resolved magnetophotoluminescence of the monolayer WS_2 on the (Ga,Mn)As films. Under a small magnetic field magnitude of 400 Oe, the circular polarization of the exciton photoluminescence is not dependent on the magnetic field (see Supplementary Section V). Circularly polarized electroluminescence was also observed on a WSe_2-based transistor controlled by the electron–hole overlap[18]. However, the creation of an unbalanced valley carrier population is key to using the valley DOF in valleytronic devices.

The experimentally observed helicity of the valley-polarized electroluminescence is limited by the efficiency of the spin-polarized carrier injection, as well as the spin and valley scattering processes in the heterostructure. Because of strong quantum confinement and weak dielectric screening in monolayer WS_2 (refs 8,9), the spin-polarized holes injected from the ferromagnetic substrate would form the valley excitons in different valleys. The valley scattering processes and depolarization of electrically populated valley excitons at non-zero temperatures contribute to reducing the contrast of the valley population[12,28,29,31]. In particular, locally increased temperature at the junction due to the Joule heating of the injected current may increase phonon-assisted intervalley scattering (see Supplementary Section VI). To accurately extract the electrical valley generation efficiency across the monolayer heterojunction, we examine the valley dynamics by time-resolved polarization measurements in the monolayer WS_2 on (Ga,Mn)As, using a synchroscan streak camera. Figure 4a displays the total photoluminescence ($\sigma-$ + $\sigma+$) intensity dynamics following a σ+ polarization from a femtosecond excitation laser pulse with an energy of 2.21 eV, tracing the exciton relaxation and recombination processes. On the basis of a two-level rate equation, we can infer an effective exciton lifetime (τ) of 2.5 ps (determined from two exciton lifetimes of 2.9 and 20.0 ps, from convolution fitting with the incident laser pulse). In addition, the time-resolved σ+ emission from the K′ valley displays a higher intensity than that of the σ– emission from the K valley (Fig. 4b), confirming the valley-contrasting selection rule. Compared with the σ+ emission, the σ– emission always decays slowly until the populations in the two valleys are equal. This difference between the two decay trends results from intervalley scattering, which tends to equalize the exciton populations in the two valleys. From convolution fitting with the incident laser pulse and recombination time as obtained above, we estimate the lifetime of intervalley scattering (τ_K) to be 2.5 ps (inset of Fig. 4b). According to the rate model and knowledge of the valley carrier dynamics[32], we can estimate the initial electrically generated valley polarization ρ_0. The degree of electroluminescence polarization ρ depends on the steady values of the valley exciton densities, N_K and $N_{K'}$, as $\rho = (N_K - N_{K'})/(N_K + N_{K'}) = (\rho_0)/(1 + 2\tau/\tau_K)$. Given the measured electroluminescence polarization of ~15%, a significant portion (~45%) of the overall valley generation efficiency remains intact across the monolayer heterojunction, consistent with previous studies using (Ga,Mn)As as the spin aligner[26].

Electrical generation and control of the valley population is at the heart of the emerging valleytronics. We experimentally demonstrate the first electrical valley polarization with spin injection from a ferromagnetic semiconductor, which is confirmed through the observed valley-polarized light emission. The electrical control of the valley DOF opens the door towards a new paradigm of electronics that manifests all three DOFs—charge, spin, and valley—for information processing and computing.

Methods

Methods and any associated references are available in the online version of the paper.

Received 28 January 2015; accepted 24 February 2016; published online 4 April 2016

References

1. Ali, M. N. *et al.* Large, non-saturating magnetoresistance in WTe_2. *Nature* **514,** 205–208 (2014).
2. Cao, T. *et al.* Valley-selective circular dichroism of monolayer molybdenum disulphide. *Nature Commun.* **3,** 887 (2012).
3. Zeng, H., Dai, J., Yao, W., Xiao, D. & Cui, X. Valley polarization in MoS_2 monolayers by optical pumping. *Nature Nanotech.* **7,** 490–493 (2012).
4. Mak, K. F., He, K., Shan, J. & Heinz, T. F. Control of valley polarization in monolayer MoS_2 by optical helicity. *Nature Nanotech.* **7,** 494–498 (2012).
5. Yao, W., Xiao, D. & Niu, Q. Valley-dependent optoelectronics from inversion symmetry breaking. *Phys. Rev. B* **77,** 235406 (2008).
6. Xiao, D., Liu, G. B., Feng, W., Xu, X. & Yao, W. Coupled spin and valley physics in monolayer of MoS_2 and other group-VI dichalcogenides. *Phys. Rev. Lett.* **108,** 196802 (2012).
7. Zhu, B., Chen, X. & Cui, X. Exciton binding energy of monolayer WS_2. *Sci. Rep.* **5,** 9218 (2015).
8. Ye, Z. *et al.* Probing excitonic dark states in single-layer tungsten disulfide. *Nature* **513,** 214–218 (2014).
9. Chernikov, A. *et al.* Exciton binding energy and nonhydrogenic Rydberg series in monolayer WS_2. *Phys. Rev. Lett.* **113,** 076802 (2014).

10. Mak, K. F., Lee, C., Hone, J., Shan, J. & Heinz, T. F. Atomically thin MoS_2: a new direct-gap semiconductor. *Phys. Rev. Lett.* **105,** 136805 (2010).
11. Splendiani, A. *et al.* Emerging photoluminescence in monolayer MoS_2. *Nano Lett.* **10,** 1271–1275 (2010).
12. Lagarde, D. *et al.* Carrier and polarization dynamics in monolayer MoS_2. *Phys. Rev. Lett.* **112,** 047401 (2014).
13. Xu, X., Yao, W., Xiao, D. & Heinz, T. F. Spin and pseudospins in layered transition metal dichalcogenides. *Nature Phys.* **10,** 343–350 (2014).
14. Ovchinnkov, D., Allain, A., Huang, Y., Dumcenco, D. & Kis, A. Electrical transport properties of single-layer WS_2. *ACS Nano* **8,** 8174–8181 (2014).
15. Ross, J. S. *et al.* Electrically tunable excitonic light-emitting diodes based on monolayer WSe_2 p–n junctions. *Nature Nanotech.* **9,** 268–272 (2014).
16. Baugher, B. W. H., Churchill, H. O. H., Yang, Y. & Jarillo-Herrero, P. Optoelectronic devices based on electrically tunable p–n diodes in a monolayer dichalcogenide. *Nature Nanotech.* **9,** 262–267 (2014).
17. Pospischil, A., Furchi, M. M. & Mueller, T. Solar-energy conversion and light emission in an atomic monolayer p–n diode. *Nature Nanotech.* **9,** 257–161 (2014).
18. Zhang, Y. J., Oka, T., Suzuki, R., Ye, J. T. & Iwasa, Y. Electrically switchable chiral light-emitting transistor. *Science* **344,** 725–728 (2014).
19. Cheng, R. *et al.* Electroluminescence and photocurrent generation from atomically sharp WSe_2/MoS_2 heterojunction p–n diodes. *Nano Lett.* **14,** 5590–5597 (2014).
20. Cheiwchanchamnangij, T. & Lambrecht, W. R. L. Quasiparticle band structure calculation of monolayer, bilayer, and bulk MoS_2. *Phys. Rev. B* **85,** 205302 (2012).
21. Ross, J. S. *et al.* Electrical control of neutral and charged excitons in a monolayer semiconductor. *Nature Commun.* **4,** 1474 (2013).
22. Zhang, Y. *et al.* Direct observation of the transition from indirect to direct bandgap in atomically thin epitaxial $MoSe_2$. *Nature Nanotech.* **9,** 111–115 (2014).
23. Korn, T., Heydrich, S., Hirmer, M., Schmutzler, J. & Schüller, C. Low-temperature photocarrier dynamics in monolayer MoS_2. *Appl. Phys. Lett.* **99,** 102109 (2011).
24. Ohno, Y. *et al.* Electrical spin injection in a ferromagnetic semiconductor heterostructure. *Nature* **402,** 790–792 (1999).
25. Flederling, R. *et al.* Injection and detection of a spin-polarized current in a light-emitting diode. *Nature* **402,** 787–790 (1999).
26. Ghosh, S. & Bhattacharya, P. Surface-emitting spin polarized $In_{0.4}Ga_{0.6}As/GaAs$ quantum-dot light-emitting diode. *Appl. Phys. Lett.* **80,** 658–660 (2002).
27. Chen, L. *et al.* Easy axis reorientation and magneto-crystalline anisotropic resistance of tensile strained (Ga,Mn)As films. *J. Magn. Magn. Mater.* **322,** 3250–3254 (2010).
28. Kioseoglou, G. *et al.* Valley polarization and intervalley scattering in monolayer MoS_2. *Appl. Phys. Lett.* **101,** 221907 (2012).
29. Yu, T. & Wu, W. Valley depolarization due to intervalley and intravalley electron–hole exchange interactions in monolayer MoS_2. *Phys. Rev. B* **89,** 205303 (2014).
30. Olejník, K. *et al.* Enhanced annealing, high Curie temperature, and low-voltage gating in (Ga,Mn)As: A surface oxide control study. *Phys. Rev. B* **78,** 054403 (2008).
31. Wang, Q. *et al.* Valley carrier dynamics in monolayer molybdenum disulfide from helicity-resolved ultrafast pump-probe spectroscopy. *ACS Nano* **7,** 11087–11093 (2013).
32. Zhu, B., Zeng, H., Dai, J., Gong, Z. & Cui, X. Anomalously robust valley polarization and valley coherence in bilayer WS_2. *Proc. Natl Acad. Sci. USA* **111,** 11606–11611 (2014).

Acknowledgements

The authors acknowledge financial support from Office of Naval Research Multidisciplinary University Research Initiative program under grant no. N00014-13-1-0649, and National Science Foundation (EFMA-1542741). J.Z. and H.W. acknowledge support from MOST of China (grant no. 2015CB921503) and NSFC (grant no. 61334006). Y.Y. thanks T. Cao of the University of California, Berkeley for helpful discussions.

Author contributions

Y.Y., X.Y., Z.Y. and X.Z. conceived the project. H.W. and J.Z. grew and characterized (Ga,Mn)As films. Y.Y., H.Z. and M.Z. developed the sample design and fabricated the samples. Y.Y., J.X. and Z.Y. performed the measurements. Y.Y. and J.X. carried out the data analysis. Y.Y., X.Y. and J.X. wrote the manuscript. X.Z., X.Y. and Y.W. guided the research. All authors discussed the results and commented on the manuscript.

Additional information

Supplementary information is available in the online version of the paper. Reprints and permissions information is available online at www.nature.com/reprints. Correspondence and requests for materials should be addressed to X.Z.

Competing financial interests

The authors declare no competing financial interests.

Methods

Growth and characteristics of (Ga,Mn)As films. The perpendicularly magnetized (Ga,Mn)As films were grown on a stain-relaxed $In_{0.17}Ga_{0.83}As$ buffer layer by molecular beam epitaxy. Standard effusion cells supplied fluxes of Ga, Mn, In, and As_4. The (Ga,Mn)As film was characterized by a superconducting quantum interference device magnetometer, indicating that the magnetic easy axis is perpendicular to the sample surface and the Curie temperature of the sample is about 150 K.

Device fabrication. First a photoresist (I-line) pattern was lithographically defined on a perpendicularly magnetized (Ga,Mn)As film as an etching mask. The (Ga,Mn)As was then defined into a mesa shape by wet etching in a solution of H_3PO_4:H_2O_2:H_2O = 1:1:38, which has an etching rate of about 2 nm s^{-1}. To prevent substrate leakages, a thin film of SiO_2 was deposited by electron beam evaporation, followed by a lift-off process. Then a site-specific dry transfer technique was used to precisely place the exfoliated monolayer WS_2 (2D semiconductors) on the interface between the SiO_2 and (Ga,Mn)As. The An In/Au (10/80 nm) electrode was then defined by electron beam lithography, followed by thermal evaporation and lift-off processes, to form an ohmic contact on the monolayer WS_2.

Electroluminescence measurements. For the electroluminescence measurements, the heterojunction device was placed in a cryogenic chamber (Janis ST 500), with the magnetic field direction perpendicular to the device surface modulated by a Helmholtz coil. The electroluminescence device was powered by a Keithley 2635A source meter. The electroluminescence spectra were captured by a 50× (0.55 NA) objective and recorded by a spectrometer (Shamrock SR-303i). To investigate the dependence of the magnetic field on helicity, the electroluminescence was modulated by a chopper and a photoelastic modulator operating at 1.6 kHz and 50 kHz, respectively, and detected by a Hamamatsu (H7422-50) GaAs photomultiplier tube with double lock-in method.